NASA TECHNICAL NOTE

NASA TN D-3347

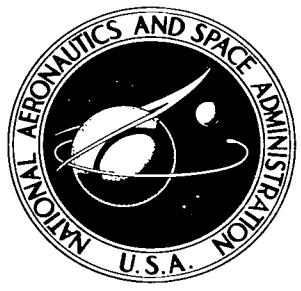

NASA TN D-3347

STEADY-STATE INVESTIGATION OF LAMINAR-FLOW INSTABILITY PROBLEM RESULTING FROM RELATIVELY LARGE INCREASES IN TEMPERATURE OF NORMAL HYDROGEN GAS FLOWING IN SMALL DIAMETER HEATED TUBE

by George E. Turney, John M. Smith, and Albert J. Juhasz

Lewis Research Center
Cleveland, Ohio

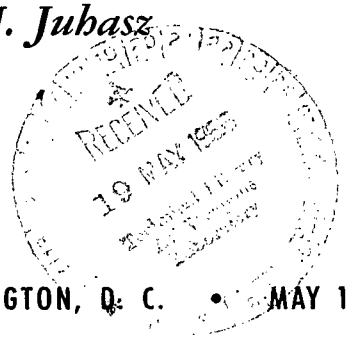

NATIONAL AERONAUTICS AND SPACE ADMINISTRATION • WASHINGTON, D. C. • MAY 1966

NASA TN D-3347

STEADY-STATE INVESTIGATION OF LAMINAR-FLOW INSTABILITY PROBLEM RESULTING FROM RELATIVELY LARGE INCREASES IN TEMPERATURE OF NORMAL HYDROGEN GAS FLOWING IN SMALL DIAMETER HEATED TUBE

By George E. Turney, John M. Smith, and Albert J. Juhasz

Lewis Research Center
Cleveland, Ohio

NATIONAL AERONAUTICS AND SPACE ADMINISTRATION

For sale by the Clearinghouse for Federal Scientific and Technical Information
Springfield, Virginia 22151 – Price $2.00

STEADY-STATE INVESTIGATION OF LAMINAR-FLOW INSTABILITY PROBLEM RESULTING FROM RELATIVELY LARGE INCREASES IN TEMPERATURE OF NORMAL HYDROGEN GAS FLOWING IN SMALL DIAMETER HEATED TUBE

by George E. Turney, John M. Smith, and Albert J. Juhasz

Lewis Research Center

SUMMARY

During certain phases of nuclear rocket operation, namely startup and shutdown, flow of hydrogen gas in the reactor core passages may change from turbulent to laminar flow as a result of fluid temperature increases in the passages. Experimental data required to validate assumptions used to estimate the pressure-drop characteristics of heated flow channels operating in (or near) the laminar-turbulent flow transition region appear to be lacking.

This report presents results from an experimental investigation conducted to determine the pressure-drop characteristics of normal hydrogen gas flowing through an electrically heated test section operating in the transition region of laminar-turbulent flow. The experimental investigation was conducted at average operating heat flux values of 0.320, 0.485, and 0.640 Btu/(sec)(ft^2). The Reynolds numbers (based on inlet conditions) ranged from approximately 600 to 5400, and the ratio of outlet to inlet fluid temperatures ranged from approximately 2.5 to 11.0. The test section used in these experiments was a Nichrome-V tube with an inside diameter of 0.116 inch and a heated length of approximately 50 inches.

From the experimental data, a steady-state curve of pressure drop as a function of inlet Reynolds number was obtained for each operating heat flux value. These curves are concave upward; the inlet Reynolds number corresponding to the point of minimum pressure drop ranged from approximately 1800 at the minimum operating heat flux of 0.320 Btu/(sec)(ft^2) to 2300 at the maximum heat flux of 0.640 Btu/(sec)(ft^2).

A comparison was made between the experimental and analytically calculated values of pressure drop for several of the test runs. With the exception of a few points, the experimental and calculated pressure drops for all test runs agreed within ±10 percent.

INTRODUCTION

The efficient application of nuclear power for rocket propulsion requires a compact high-power-density reactor in which the propellant gas (hydrogen) is heated to extremely high temperatures. In the homogeneous reactor core proposed for the nuclear rocket, the heat generated in the solid fuel element array is removed by the hydrogen propellant that flows axially through hundreds of small-diameter, parallel coolant passages in the core. A typical fuel element coolant passage design for the nuclear rocket core is depicted in reference 1.

In a parallel flow system of the type described in reference 1, the static pressure drop across each flow channel in the core is set by the inlet and exit plenum pressures; that is, the static pressure drop across all flow channels must be identical and equal to the pressure difference from inlet to exit plenum. In such a system, nonuniform flow distributions among the hundreds of parallel coolant passages could result from a variety of conditions, (e.g., dimensional differences among the passages, nonuniform spatial heat generation rates, etc.) and could place a serious limit on the design performance of the nuclear propulsion system.

During certain phases of nuclear rocket operation, flow of hydrogen gas through the parallel passages of the reactor core may lead to any one of several distinct flow problems. For steady-state operation with no heat addition, the pressure drop in the passages is an increasing function of the flow rate in both the laminar and turbulent flow regimes; that is, the pressure-drop flow-rate curve has a positive slope in the laminar and turbulent flow regimes. For laminar flow with constant heat addition, however, the slope of the steady-state pressure drop - flow rate curve may be either positive or negative, depending on the value of the outlet-to-inlet fluid temperature ratio in the heated passage. The outlet-to-inlet fluid temperature ratio at which the slope of the laminar-flow pressure-drop flow-rate curve changes from positive to negative is herein termed the "critical fluid temperature ratio." For values of outlet-to-inlet gas temperature ratio greater than critical, the steady-state pressure-drop flow-rate curve exhibits a negative resistance to flow (i.e., a negative slope). For values of the temperature ratio less than critical, the slope of the steady-state pressure-drop flow-rate curve is positive. Hence, with a constant rate of heat input, the characteristic pressure-drop flow-rate curve with laminar flow is U-shaped (i.e., concave upward, with a minimum pressure drop occurring at the critical fluid temperature ratio).

Increases in the heat addition rate have been shown to result in other U-shaped pressure-drop flow-rate curves that exhibit the following characteristics: for a given pressure drop, the flow rate for the left leg of the U-shaped curve increases, and that for the right leg decreases as the heat flux is increased. If a small perturbation in heat flux is imposed, the flow rate for both legs tends to decrease. For the left leg, this tendency is in opposition to the steady-state trend. These phenomena have been widely termed the "laminar flow instability problem" and will be discussed in more detail in the section GENERAL DISCUSSION OF PROBLEM.

Analytical studies of the laminar flow of gases through heated tubes have been made by numerous investigators, especially since the start of the development of nuclear rockets. Some of these studies are reported in references 2, 3, and 4. In each case, the analytical results are in agreement with the discussion presented in the preceding paragraph. An experimental study of the laminar flow of helium through a heated capillary tube (0.012-in. i.d.) is reported in reference 5. With a constant electrical heat input to this capillary, the experimental data of reference 5 indicate the existence of two widely different laminar flow rates for a fixed value of pressure drop in the capillary.

During nuclear rocket flight, two distinct operating periods must be examined from the laminar instability viewpoint. The first, startup, may not be of significance if the period of low flow operation is traversed rapidly. The second, shutdown, may conceivably lead to serious difficulties, depending on the method of cooling employed to remove afterheat. One proposed scheme for removing the reactor afterheat involves pulse cooling; the use of pulses of appropriate strength and spacing may make it possible to maintain turbulent flow and, hence, stability. The cost of pulse cooling from a propellant standpoint depends directly on the mission intended for the nuclear rocket; whether or not this cost may be prohibitive cannot be stated at this time.

A second method for removal of reactor afterheat may involve a continuous flow of coolant at an average rate which may be considerably smaller than that required for pulse cooling. If this scheme is employed, it is almost assured that at some time following shutdown mixed flow would exist in the reactor core; that is, as a result of fluid viscosity increases with increases in temperature, turbulent flow would enter the passage and laminar flow would leave the passage.

A transition of this type (complete turbulent flow to complete laminar flow) would be expected to occur gradually over a length of flow passage equivalent to several tube diameters. Experimental data describing or defining the nature of a flow transition of this type appears to be lacking in the literature. Consequently, the number of tube diameters required for a complete flow transition to occur in a heated flow channel operating in the transition flow regime is uncertain. In addition, the value of the local bulk Reynolds number at which a flow transition of this type begins is also somewhat uncertain.

In order to study the steady-state pressure-drop flow-rate characteristics of this type of flow in a passage the size of those currently used in the nuclear rocket cores and for flow conditions anticipated during reactor afterheat removal, an analytical parametric study was conducted at the Lewis Research Center and is reported in reference 6. The study is dependent on an assumed laminar-turbulent flow transition criterion. For this study, flow was considered laminar at Reynolds numbers up to 2100 and turbulent down to about 1000. In other words, a laminar flow remains laminar until the Reynolds number exceeds 2100, and turbulent flow remains turbulent until the friction factor in laminar flow is larger than that in turbulent flow. In the study

reported in reference 6, constant axial heat input was also assumed. The laminar-flow friction factor from the Poiseuille equation (ref. 7) and the Kármán-Nikuradse formulation for use in turbulent flow with high film-to-bulk temperature ratios (ref. 7) were used in this analysis. Since the Reynolds number was based on film properties, wall temperatures had to be computed; these calculations were based on the assumption that the power generated in the solid is all transferred to the fluid. Furthermore, both laminar and turbulent heat-transfer correlations had to be employed.

Calculations presented in reference 6 demonstrate that a minimum pressure drop always exists in a mixed flow passage. The value of the minimum pressure drop increases with heat input.

In an effort to study in more detail the rather uncertain transition region between laminar and turbulent flow, that is, to determine the pressure-drop flow-rate characteristics and the relative position of the minimum steady-state pressure drop point, an experimental investigation was conducted at the Lewis Research Center with normal hydrogen gas flowing through an electrically heated 0.116-inch-diameter Nichrome-V tube. This steady-state single-tube test marks only an initial step in a program of flow study through a nuclear rocket core. The purpose of this report is to present the experimental results of the initial phase of the overall program and compare these experimental results with theoretical predictions. The steady-state operating conditions covered in this first-phase investigation reported herein are as follows: inlet Reynolds numbers from 600 to 5400, outlet-to-inlet gas temperature ratios from 2.5 to about 11.0, and average heat fluxes of 0.320, 0.485, and 0.640 $Btu/(sec)(ft^2)$.

To determine reproducibility of the experimental results, tests for similar operating conditions were run three times. Results of the initial runs were reported in reference 8. Results from the two sets of reruns, together with the initial run results, are presented herein.

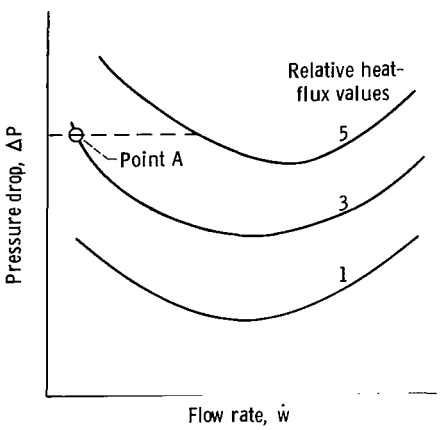

Figure 1. - Static pressure drop in heated flow passage with laminar flow as function of flow rate for various relative heat-flux values.

GENERAL DISCUSSION OF PROBLEM

Steady State

From an examination of the steady-state equations of static pressure-drop for laminar flow in a uniformly heated flow passage, it can be shown that two different flow rates are possible for a given value of pressure-drop in the flow passage. This phenomenon is illustrated in figure 1, where the pressure-drop in the flow passage ΔP is shown as a function of the coolant channel flow rate $\dot{w}$ for various relative heat flux values. (All symbols are defined in appendix A.)

A derivation and general analysis of the

equation for static pressure drop of an ideal gas flowing in a constant area passage with constant, uniform axial heat input is presented in appendix B.

The resulting steady-state expression for static pressure drop in a constant area passage with an assumed constant and uniform axial heat input (eq. (1) of appendix B) is

$$\Delta P_{s,1-2} = \frac{2R}{g}\frac{T_1}{P_1 + P_2}\left(\frac{\dot{w}}{A}\right)^2\left\{\frac{4QL}{A_s C_p D_H T_1 \frac{\dot{w}}{A}} + \frac{2}{D_H}\frac{f_o \mu_1^n L}{(Mn+2)\left(\frac{\dot{w} D_H}{A}\right)^n}\right.$$

$$\left.\times \frac{A_s C_p D_H T_1 \frac{\dot{w}}{A}}{4QL}\left[\left(1 + \frac{4QL}{A_s C_p D_H T_1 \frac{\dot{w}}{A}}\right)^{Mn+2} - 1\right]\right\} \qquad (1)$$

The characteristic concave upward shape of the curves in figure 1 can be demonstrated from an analysis of equation 1. In appendix B, this equation is analyzed, and the following general conclusions are drawn:

(1) With the heat input to the fluid approaching zero (i.e., with $Q \to 0$) such that the flow is essentially adiabatic, the static pressure drop $\Delta P_{s,1-2}$ is an increasing function of flow rate $\dot{w}$ in both the laminar- and turbulent-flow regimes.

(2) With a constant and uniform finite heat input to the fluid, however, the static pressure drop may be either an increasing or decreasing function of flow rate:

(a) For the case in which the flow is turbulent throughout the passage (i.e., for Reynolds numbers >2100) the static pressure drop $\Delta P_{s,1-2}$ increases with flow rate $\dot{w}$ for all values of heat input.

(b) For the case in which the flow is laminar throughout the passage (i.e., for Reynolds numbers <2100) the static pressure-drop $\Delta P_{s,1-2}$ decreases with flow rate provided the heat input is sufficient to yield an outlet-to-inlet fluid temperature ratio which exceeds τ_{crit}.

The critical fluid temperature ratio τ_{crit} for laminar flow of normal hydrogen gas in a uniformly heated passage having a length and diameter approximately equal to a nuclear rocket core passage was determined by examining equation (1) for extreme values. A relative minimum pressure drop was found to correspond to a critical fluid temperature ratio of approximately 4.0. The procedure used to calculate the critical fluid temperature ratio for laminar flow of normal hydrogen gas is described in appendix B.

The analysis presented in appendix B is considered approximate in nature. As pointed out, the derivation of the static pressure-drop equation (eq. (1)) was based on several simplifying assumptions. It should also be recognized

that the computed critical fluid temperature ratio (of approx. 4.0) for all laminar flow was based on the assumption that the heat input was constant and uniform along the axis of the passage. It is expected that the value of τ_{crit} would be somewhat different if the axial heat-flux distribution were nonuniform.

Nonsteady State

The transient facet of the laminar flow instability problem is that which applies to the stability of a heated flow channel to perturbations when operating at a point on the steady-state pressure-drop flow-rate curve where the slope of the curve is negative.

With reference to figure 1, it appears from the steady-state pressure-drop relations that if an operating point is chosen in the regime of negative slope (e.g., point A in fig. 1) and the heat flux is increased slightly by an amount dQ, the flow rate $\dot{w}$ must increase if the pressure-drop ΔP is fixed. An analysis of the transient behavior of a heated flow channel does not, however, lead to this conclusion.

If ΔP is fixed (as would be the case in the multichannel parallel flow system with fixed pressure boundaries) and the heat flux in one channel of the parallel flow system is increased by an amount dQ, a decrease in $\dot{w}$ would be expected as a result of a decrease in the average fluid density in the flow passage.

Results of unpublished analytical studies indicate that the negative slope region of the steady-state pressure-drop flow-rate curve is unstable. Positive perturbations in heat input have been shown to cause a continuous unbounded divergence in flow rate from the initial steady-state flow rate. At the low operating heat fluxes which are associated with the nuclear rocket afterheat removal period, the flow divergence caused by positive heat-flux perturbations occurs at a relatively slow rate and is accompanied by a continuously increasing flow passage surface temperature. The calculated unbounded flow-rate divergence associated with positive perturbations in heat input is based on the assumptions that the heat input to the passage is constant and that heat conduction from the passage is insignificant.

The effect of heat interchange by conduction in the solid material of the reactor core would tend to prevent a continuing increase in temperature in those flow channels that are affected by an induced positive perturbation in heat input.

The uncertainty in the conduction contact resistance between the solid fuel modules in the reactor core, however, makes it impossible to accurately determine the effectiveness of heat conduction in reducing the magnitude of nonuniformities in temperature and flow which might result from this phenomenon.

From the previous discussion, it appears that laminar flow in the passages of the nuclear reactor core could present a serious problem, particularly during

the period of low power operation which follows a shutdown of the nuclear rocket reactor.

In the single-passage flow experiment described in this report, the laminar-flow perturbation instability problem was not encountered because of the relatively large flow impedance added into the system by the flow and pressure control valves. The pressure losses across these valves were relatively large compared with the pressure losses in the heated tube. As a result, the control valves had a stabilizing influence on the flow rate in the test system.

Since the perturbation instability problem was not considered as an objective in this experimental investigation, no further discussion of that facet of the problem will be made.

EXPERIMENTAL APPARATUS AND PROCEDURE

Test Assembly

A sketch of the experimental setup is shown in figure 2. The hydrogen gas used in these experiments was supplied from a tube trailer, metered by calibrated rotameters, and precooled by a liquid nitrogen heat exchanger prior to entering the heated test section. The test section for these experiments was a Nichrome-V tube with an inside diameter of 0.116 inch, a wall thickness of 0.016 inch, and a heated length of 50 inches. The electrical resistivity of Nichrome-V at several temperatures from 70° to 2000° F is shown in table I. From an inspection of table I, it is seen that the resistivity of Nichrome-V is large and relatively constant over a wide range of temperatures.

Two electrical power systems were used independently to supply power to the test section. In the initial set of test runs, the test section was heated by a manually controlled 6-kilovolt-ampere alternating-current power supply. For the two sets of reruns, a direct-current power supply with an automatic temperature feedback control was used. (It was mentioned previously that three separate sets of experimental data were taken for each operating heat flux. The primary purpose of running the two additional sets of data was to determine the reproducibility of the experimental measurements.) The direct-current power supply with automatic control was used to facilitate the setting up of the required power input for the reruns. The fact that two different types of electrical power were used (ac and dc) should have no effect on the measured data.

The approximate positions of the electrical power connections are shown schematically in figure 2. To reduce heat sink effects, the electrical power tap on the downstream side of the heated test section was positioned just above the stainless-steel outlet plenum. Because of the large cross-sectional area of the outlet plenum, the electrical power dissipated in the plenum was relatively insignificant. (It was estimated that the power dissipated in the outlet plenum was less than 0.1 percent of the electrical power input.) The power tap at the test section inlet was located just above the liquid nitrogen heat exchanger and approximately 1.5 inches above the test section inlet.

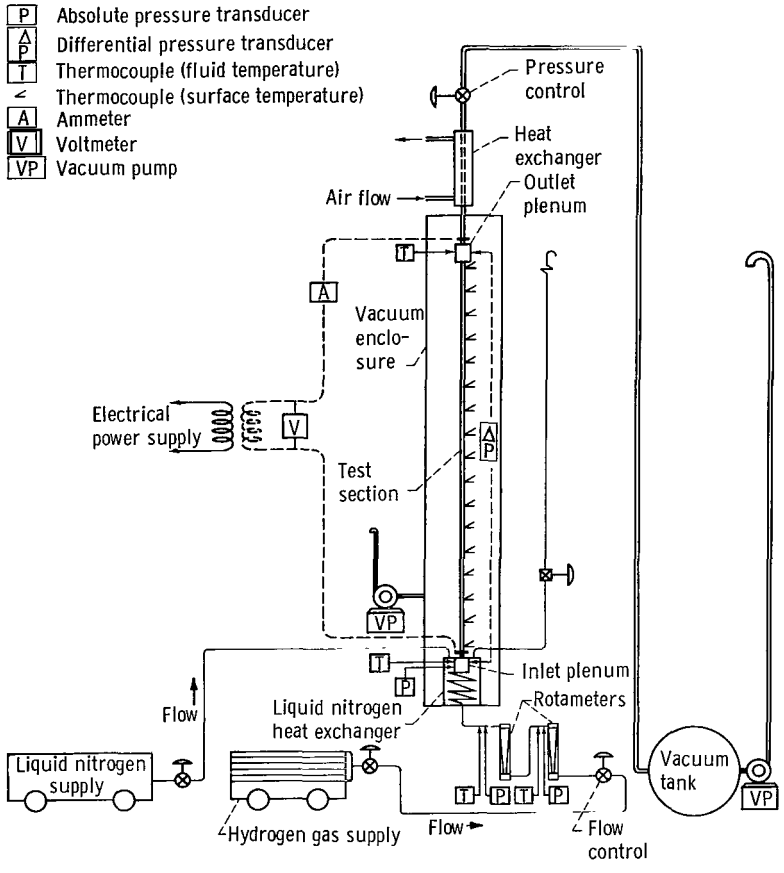

Figure 2. - Schematic diagram of test assembly and instrumentation.

TABLE I. - ELECTRICAL RESISTIVITY OF NICHROME-V AT SEVERAL TEMPERATURES

[Data obtained from Driver-Harris Co. Technical Catalog, NCR58.]

Temperature, °F	Resistivity, (ohm)(circular mils)/ft
70	650.0
200	660.5
400	674.0
600	685.0
800	693.0
1000	696.0
1200	692.0
1400	690.0
1600	693.0
1800	697.0
2000	701.0

In order to minimize heat losses by free convection, the test assembly was enclosed in an evacuated chamber, which was maintained at an absolute pressure of approximately 10^{-2} millimeter of mercury. The heated fluid leaving the test section was cooled by a single-pass air-cooled heat exchanger and exhausted into a vacuum tank. The purpose of exhausting to the vacuum tank was to enable the testing to be conducted at a subatmospheric pressure level; this was considered necessary to maximize the pressure drop across the heated test section.

Figure 3 is a photograph of the test assembly showing the position of the Nichrome-V test section inside the vacuum enclosure.

Instrumentation

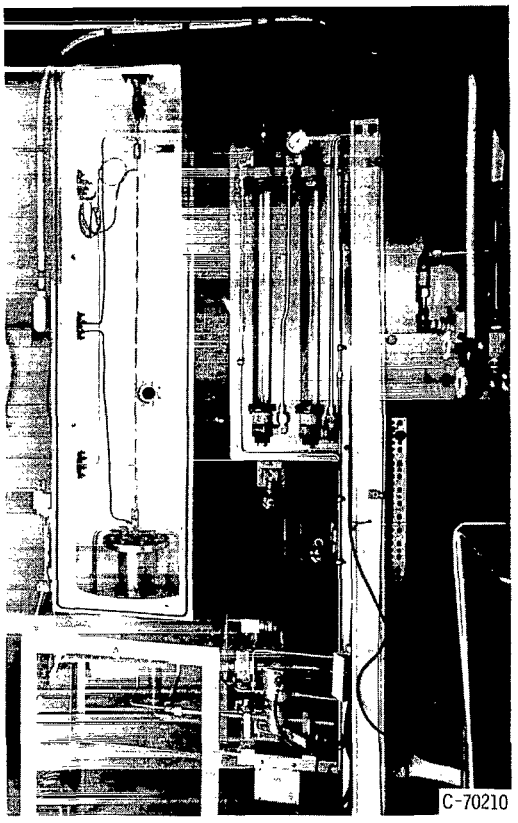

Figure 3. - Photograph of test assembly.

The relative locations and types of instrumentation used on the test assembly are indicated schematically in figure 2. The hydrogen flow rate was measured by two rotameters, each having a different range, connected in series and located in the flow line upstream of the test section. The rotameters were read remotely on a closed-circuit television receiver.

The Nichrome-V test section was instrumented with 36-gage (0.005-in.-diam.) iron-Constantan thermocouples, which were bonded to, and electrically insulated from, the outside surface of the test section by a thin layer of ceramic cement. A total of 17 thermocouples, spaced 3 inches apart, were positioned along the middle 48 inches of the 50-inch-long heated length of tube. In order to minimize the conduction error in the wall temperature measurements, two turns of the insulated thermocouple lead wires were wrapped around and bonded to the surface of the heated tube at each measurement point. (During the testing, however, some of these thermocouples became detached or failed. As a result, wall temperature data were not obtained for each test run.)

The temperature of the hydrogen gas at the inlet and outlet plenums was measured by thermocouples positioned inside the plenums. A copper-Constantan thermocouple was used in the inlet plenum and an iron-Constantan thermocouple, surrounded with a stainless-steel radiation shield, was used in the outlet plenum. In addition, hydrogen gas temperature measurements were made with copper-Constantan thermocouples positioned in the transfer line immediately downstream of each rotameter.

Static pressure taps were located in the plenums upstream and downstream of the test section. The pressure at the inlet plenum was measured with a transducer having a range of 12 pounds per square inch absolute (full-scale range); the pressure drop across the test section was measured with two different differential transducers having full-scale ranges of 0.7 and 0.3 pound per square inch. Pressure measurements were also taken in the transfer line immediately downstream of each rotameter. The electrical power input to the test section was determined from measurements of amperage and voltage drop across the power leads.

Precision of Experimental Measurements

The recording instruments used in this experiment were of high precision. The pressure transducers (both the differential and absolute transducers) were rated at ±1 percent of full scale. The accuracy of the thermocouples, particularly those used to measure the test section wall temperatures, is difficult to determine. It was estimated, however, that errors caused by conduction through the thermocouple lead wires were relatively small. (As mentioned previously, the thermocouple lead wires were wrapped around and bonded to the surface of the tube at each measurement point.) The rotameters used to measure the flow rates were calibrated with normal hydrogen gas; data points from the calibration were reproducible within about ±1/2 percent. It is estimated that the accuracy of the flow rate measurements were within ±3 percent.

The reproducibility of the experimental measurement is not considered to be a quantitative indication of accuracy. Nevertheless, reproduction does provide a basis for confidence in the test results. For the most part, the reproducibility of the test data was reasonably good.

Experimental Procedure

For each steady-state test run, the static pressure and temperature at the test section inlet were maintained constant at approximately 10 pounds per square inch absolute and 140° R, respectively. The required flow rate for each run and the constant value of inlet pressure was established by opening the pressure and flow control valves to a proper setting. The electrical power input to the test section was then adjusted (either manually with the ac power supply or automatically with the dc power supply) to give an outlet fluid temperature for the established flow rate, which corresponded to a predetermined constant heat flux value. When the system reached steady state (i.e., when equilibrium temperatures and pressures were reached for the established flow rate) the experimental data were recorded. For the initial test runs, a continuous 30-second analog recording of the data was made for each test condition. These data were taken on an automatic frequency-modulated tape recorder, processed, and played back on strip charts by a pen-type oscillograph. The analog data acquisition and the play-back system are described in reference 9. For the two sets of reruns, the experimental pressure measurements were recorded on strip-chart recorders, and temperature measurements were displayed on a digital voltmeter.

Experimental investigations were made for three nominal values of operating heat flux (0.320, 0.485, and 0.640 Btu/(sec)(ft^2)). For each test run, the inlet fluid temperature T_1 was maintained constant (within ±1° R) at 140° R. The operating conditions for each of the three nominal heat flux values were determined prior to running the experiments. For each nominal heat flux, several values of flow rate were specified, and the corresponding values of outlet fluid temperatures (required to give the nominal values of heat flux) were determined from the following equation:

$$\frac{Q}{A_s} = \frac{\dot{w}}{A_s} \int_{T_{1=140^{\circ}R}}^{T_2} C_p \, dT \qquad (2)$$

In running the experiments, some difficulty was encountered in establishing the exact values of the specified flow rates and corresponding outlet fluid temperatures. For some of the test runs, the measured values of $\dot{w}$ and T_2 were found to be slightly different from those computed prior to testing. Consequently, the actual Q/A_s values (computed by use of equation (2) from the experimentally measured values of $\dot{w}$ and T_2) differed slightly from the reported nominal values. The actual Q/A_s values for the individual test runs were determined and will be presented in the section RESULTS AND DISCUSSION.

Because of heat losses from the test section by radiation to the enclosure, and, to a lesser extent, by conduction from the inlet and outlet ends of the test section, the electrical power input could not be used as a measure of the average heat flux.

PRESSURE-DROP ANALYSIS

An estimate of the pressure drop in the heated passage was made for several of the experimental runs. Since the axial heat-flux distributions for the individual test runs were apparently nonuniform, especially for those runs made at the higher operating temperatures, the fluid temperature profiles required for a pressure-drop analysis could not be computed directly from equation (2). (Fluid temperature measurements were made only at the inlet and outlet of the test section.) Therefore, the experimental wall temperature profiles (to be discussed in the section RESULTS AND DISCUSSION) were used with appropriate convection heat-transfer relations to estimate the fluid temperature profiles and heat-flux profiles for the individual test runs.

The estimated fluid temperature profiles were used in the analysis to compute the pressure drops across the heated test section for these test runs. The procedure used to calculate the pressure drops consisted of dividing the total test section length into 26 equal segments, each of length Δx, and computing the static pressure drop in each segment of the heated tube from inlet plenum to exit plenum. (The total length of the Nichrome-V tube, including the $1\frac{1}{2}$-in. entrance length, was $51\frac{1}{2}$ in.; hence, Δx was approx. 2.0 in.) The pressure drops for the individual test runs were computed from the following equation:

$$\Delta P_{s,1-2} = \sum_{x=0}^{L} \left[2\left(\frac{\dot{w}}{A}\right)^2 \frac{R}{g} \frac{1}{P_x + P_{x+\Delta x}} \left(T_{x+\Delta x} - T_x + \frac{2}{D_H} \int_x^{x+\Delta x} fT \, dx \right) \right] \qquad (3)$$

The numerical operations required to compute the pressure drops from equation (3) were performed on a high-speed digital computer. (Equation (3) is essentially the same as equation (B4) of appendix B. It is written in a somewhat different form herein as a convenience for use on the digital computing machine.) The flow rates, inlet fluid temperatures and pressures used in equation (3) were obtained from the experimental measurements.

For many of the test runs analyzed, the flow entering the heated tube was turbulent. As a result of fluid temperature increases along the tube length, the flow changed to laminar flow (based on local bulk Reynolds numbers) at some position downstream of the tube inlet.

In the analysis, an assumed turbulent-to-laminar flow transition criterion was used. For the case of turbulent flow entering the test section, (i.e., for $Re_{inlet} > 2100$) the transition from turbulent to laminar flow in the heated passage was assumed to occur at a position downstream of the passage inlet where the local bulk Reynolds number reached a value of 1000. For the case of laminar flow entering the test section $\left(\text{i.e., for } Re_{inlet} \leq 2100\right)$ the flow was considered laminar throughout provided the local bulk Reynolds number at all points in the passage was less than or equal to 2100. These flow transition criteria are the same as those described and used in reference 6. As pointed out in reference 6, the local Reynolds number transition value of 1000 for turbulent-to-laminar flow was arbitrarily assumed.

The friction factors used in the pressure-drop analysis were computed from the following relations:

(1) For laminar flow with moderate wall-to-bulk temperature differences (ref. 10)

$$f = \frac{16}{Re_b}\left(\frac{T_{wall}}{T_b}\right)^{1.35} \tag{4}$$

As stated in reference 10, the effects of heat addition together with hydraulic entrance region effects are combined in the temperature ratio term in equation (4). In appendix B, these combined effects on friction factor f were ignored, and the Poiseuille equation for isothermal laminar flow (eq. (B5)) was used.

(2) For turbulent flow in long smooth tubes (ref. 7)

$$f = 0.0014 + \frac{0.125}{Re_b^{0.32}} \tag{5}$$

Equation (5) is the Koo expression and is recommended for turbulent-flow Reynolds numbers ranging from 3×10^3 to 3×10^6. Because of the assumed transition criteria, it was necessary (in some cases) to use equation (5) for Reynolds numbers down to 10^3.

The Koo expression (eq. (5)) is somewhat different from the turbulent-flow

friction factor equation in appendix B. The Koo expression was used in this analysis primarily because it more accurately describes the friction factor curve for smooth tubes at low turbulent Reynolds numbers. The hydraulic entrance region effects with turbulent flow were determined from reference 11 to be relatively insignificant and were ignored in the analysis.

For each of the test runs analyzed, the local heat-flux values and/or fluid temperature values required to compute the static pressure drops in each axial segment (of length Δx) of the heated passage were obtained from a simultaneous solution of the following equations:

$$\left(\frac{Q}{A_s}\right)_x = h_x\left[T_{wall,x} - \left(\frac{T_{x+\Delta x/2} + T_{x-\Delta x/2}}{2}\right)\right] \tag{6}$$

$$\left(\frac{Q}{A_s}\right)_x = \left(\frac{\dot{w}}{A_s}\right)_x \int_{T_{x-\Delta x/2}}^{T_{x+\Delta x/2}} c_p \, dT \tag{7}$$

where x is the distance from the test section inlet. Values of the local heat-transfer coefficient h_x were computed from the following relations:

(1) For laminar flow (ref. 12)

$$h_x = \frac{k_b}{D_H}\left[4.36 + \frac{0.036\left(\frac{Re_{b,x}Pr_{b,x}}{x/D_H}\right)}{1 + 0.0011\left(\frac{Re_{b,x}Pr_{b,x}}{x/D_H}\right)}\right] \tag{8}$$

Equation (8) was developed analytically and is based on an assumed constant axial heat input and a calculated nonparabolic fluid velocity profile. (As described in reference 13 the fully developed laminar flow velocity profile is not parabolic when heat is added.) Equation (8) was used to compute local laminar-flow heat-transfer coefficients even though the assumption of a constant axial heat input (used in the development of eq. (8)) was not fulfilled in this experiment.

(2) For turbulent flow with moderate wall-to-bulk temperature differences (ref. 7)

$$h_x = 0.023 \frac{k_b}{D_H} Re_b^{0.8} Pr_b^{0.4}\left[1 + \left(\frac{D_H}{x}\right)^{0.7}\right] \tag{9}$$

Equation (9) is recommended for complete turbulent flow (i.e., for Reynolds numbers $> 10^4$; however, equation (9) was used in this analysis for Reynolds numbers as low as 10^3.

Since values of heat-transfer coefficient in the transition flow regime have been found to vary considerably for different flow systems, the use of equation (9) in estimating turbulent heat-transfer coefficients at low turbulent Reynolds numbers is recognized as questionable.

The assumed turbulent-to-laminar flow transition criterion used in the friction factor evaluation was also used in determining the appropriate equation for computing the local heat-transfer coefficients. The values of wall temperature $\left(T_{wall,x}\right)$ used in equation (6) to compute the local heat fluxes for the individual test runs were taken from the respective wall temperature curves.

The local fluid temperatures computed from equation (7) were used in equation (3) to determine the static pressure drop in each of the 26 axial flow segments; the computed static pressure drop from inlet to exit of the test section $\Delta P_{s,1-2}$ was obtained by summing the pressure drops in each of the flow segments. Pressure losses at the entrance and exit of the test section were included in the computed pressure drops and were estimated from the following relations:

(1) For the sudden contraction entrance pressure loss (from inlet plenum to tube)

$$\Delta P_{entrance} = 0.5 \frac{1}{144} \frac{\dot{w}^2 RT_1}{2gP_{s,1}A^2} \tag{10}$$

(2) For the sudden expansion exit pressure loss (from tube to exit plenum)

$$\Delta P_{exit} = 1.0 \frac{1}{144} \frac{\dot{w}^2 RT_2}{2gP_{s,2}A^2} \tag{11}$$

The pressure loss coefficients in equations (10) and (11) were obtained from reference 14.

Fluid properties used in the computations were taken from a digital-subroutine library of hydrogen properties. (The subroutine is described in ref. 15.) Local values of computed pressure and fluid temperature in the respective segments were used in the subroutine to evaluate the fluid properties used in the pressure drop and heat-transfer equations.

RESULTS AND DISCUSSION

Experimental Wall Temperature Data

Figure 4 shows experimental wall temperature profiles for several test runs made at each of the three average operating heat fluxes. An inspection of the wall temperature profiles shows that the axial temperature distribution for each of the three heat fluxes becomes increasingly nonlinear at the higher

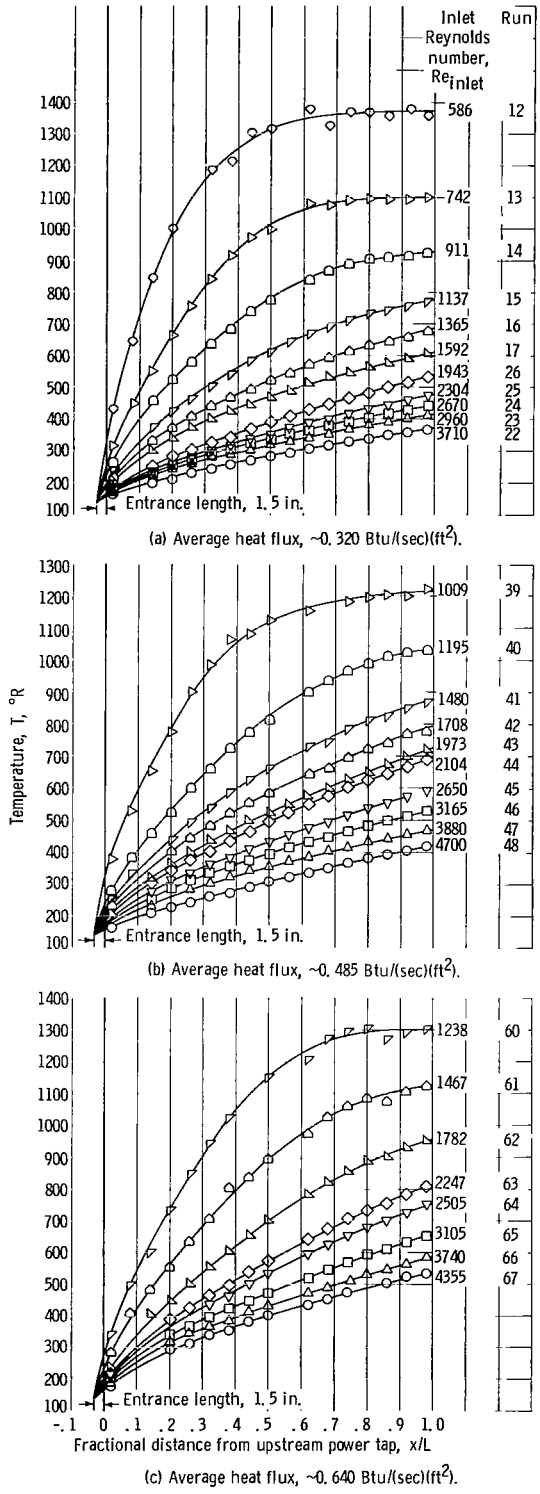

Figure 4. - Test-section wall temperature profiles for different values of inlet Reynolds number.

operating temperatures. Figure 4 shows that at the higher operating temperatures the slopes of the wall temperature curves are steep near the test-section inlet and decrease along the length of the heated tube.

Since the local slopes of the wall temperature curves are a relative indication of the local axial heat flux, it appears that for those test runs made at high operating temperatures (and/or low inlet Reynolds numbers) a major portion of the total heat input to the fluid was added in the leading half of the test section. The increasing nonlinearity of the wall temperature profiles at the higher operating temperatures can be attributed primarily to appreciable heat losses by radiation from the downstream portion of the tube surface. Therefore, even though the integrated heat input (as defined by eq. (2)) was essentially constant for each test run in a particular heat-flux series, the distribution of heat input to the fluid would be expected to be somewhat different.

Axial Heat-Flux Distributions

Figure 5 shows the calculated axial heat-flux distributions for three of the test runs made at an average operating heat flux of 0.640 Btu/(sec)(ft^2). Although the areas under each of the heat-flux curves in figure 5 are approximately the same, the distributions are seen to be vastly different. The increasing nonuniformity in heat flux with increasing operating temperatures (or decreasing inlet Reynolds numbers) is attributed primarily to significant radiation heat losses from the downstream end of the heated test section.

An examination of calculated heat-flux distributions for the other average operating heat fluxes indicates that the distributions in figure 5 are typical; that is, the calculated distributions of

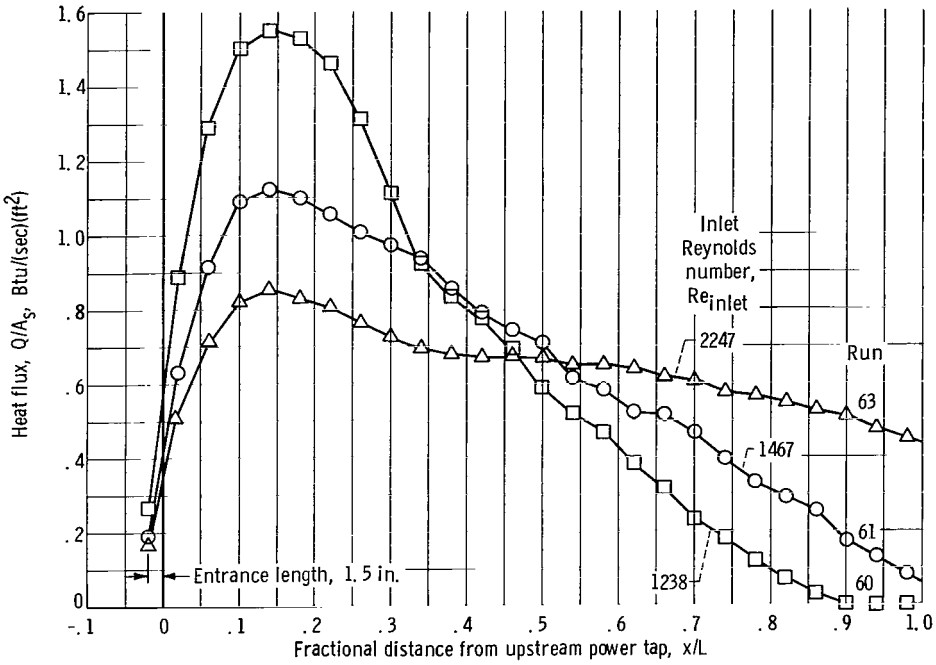

Figure 5. - Calculated heat-flux distributions along length of test section for different values of inlet Reynolds number. Average heat flux, ~0.640 Btu/(sec)(ft^2).

heat input for each operating heat flux become increasingly nonuniform with increases in operating temperature.

Experimental Pressure-Drop Flow-Rate Characteristics

The results of the laminar-flow instability experiments are presented in figure 6. The upper curves in figure 6 show the static pressure drop across the heated test section (expressed as the product of inlet pressure and static pressure drop) as a function of inlet Reynolds number for average heat-flux values of 0.320, 0.485, and 0.640 Btu/(sec)(ft^2), respectively. An inspection of the pressure-drop curves shows that the position of the relative minimum pressure drop moves upward and to the right with increasing heat flux. At the minimum operating heat flux, the relative minimum pressure drop corresponds to an inlet Reynolds number of approximately 1800; at the maximum operating heat flux, the relative minimum pressure drop corresponds to an inlet Reynolds number of approximately 2300.

The lower curves in figure 6 show the experimental outlet-to-inlet fluid temperature ratios as a function of inlet Reynolds number. An examination of these curves indicates that the fluid temperature ratio T_2/T_1 at the point of of minimum pressure drop increases from a value of 4.0 at the minimum heat flux to approximately 5.5 at the maximum heat flux.

From the analysis presented in appendix B, the value of T_2/T_1 corresponding to the point of minimum pressure drop for all laminar flow was estimated to be approximately 4.0.

TABLE II. - TEST DATA FROM HYDROGEN GAS FLOW INSTABILITY EXPERIMENTS

Run	Measured flow rate, $\dot{w}$, lb/sec	Calculated average heat flux, Q/A_s, Btu/(sec)(ft^2)	Measured inlet pressure, $P_{s,1}$, psia	Measured static pressure drop, $\Delta P_{s,1-2}$, psi	Calculated inlet Reynolds number	Measured outlet fluid temperature, T_2, $^\circ$R	Calculated fluid temperature ratio, T_2/T_1	Calculated outlet Reynolds number	Measured inlet pressure times measured static pressure drop, $P_{s,1}(\Delta P_{s,1-2})$
1	10.56×10^{-6}	0.330	10.03	0.410	605	1279	9.15	129	4.12
2	13.45	.320	10.00	.258	770	1036	7.40	188	2.58
3	15.95	.314	9.86	.220	915	900	6.43	245	2.17
4	19.70	.330	9.87	.200	1130	794	5.68	290	1.97
5	23.90	.311	9.93	.173	1370	657	4.70	457	1.72
6	27.90	.315	10.00	.166	1600	589	4.21	575	1.66
7	33.00	.319	9.90	.162	1890	534	3.82	725	1.60
8	41.85	.311	9.90	.170	2400	449	3.21	1022	1.68
9	47.80	.315	10.00	.182	2740	420	3.00	1235	1.82
10	53.50	.322	9.94	.195	3070	399	2.85	1441	1.94
11	61.00	.329	10.00	.206	3500	361	2.58	1750	2.06
12	10.21	.327	9.87	.350	586	1351	9.65	122	3.46
13	12.98	.329	9.97	.244	742	1077	7.67	170	2.43
14	15.90	.319	9.90	.199	911	913	6.52	242	1.97
15	19.84	.317	10.17	.171	1137	767	5.48	345	1.74
16	23.83	.319	10.12	.163	1365	670	4.78	449	1.65
17	27.80	.318	10.05	.158	1592	600	4.28	564	1.59
18	21.80	.320	9.87	.175	1250	718	5.12	389	1.73
19	17.50	.320	10.05	.196	1003	850	6.08	339	1.97
20	11.35	.320	9.90	.305	650	1211	8.66	138	3.02
21	33.80	.328	10.05	.160	1937	535	3.82	730	1.61
22	64.70	.311	10.00	.232	3710	349	2.49	1900	2.32
23	51.70	.312	10.00	.191	2960	397	2.83	1390	1.91
24	46.60	.314	10.00	.174	2670	424	3.03	1190	1.74
25	40.20	.311	9.99	.164	2304	463	3.31	972	1.63
26	33.90	.315	10.03	.152	1943	519	3.71	757	1.53
27	13.86	.488	9.96	.445	795	1460	10.43	157	4.43
28	14.96	.477	9.87	.401	858	1318	9.41	179	3.96
29	16.17	.471	9.87	.363	927	1243	8.88	201	3.58
30	20.91	.472	9.87	.289	1200	1004	7.17	300	2.85
31	25.80	.487	9.96	.260	1480	869	6.21	406	2.59
32	29.82	.481	9.99	.231	1710	770	5.50	508	2.31
33	34.35	.482	9.96	.222	1970	694	4.96	624	2.21
34	38.50	.480	9.88	.229	2210	636	4.54	754	2.26
35	43.40	.489	9.96	.237	2490	591	4.22	894	2.36
36	51.80	.484	10.00	.252	2970	521	3.72	1158	2.52
37	59.80	.479	9.88	.274	3430	472	3.37	1420	2.70
38	75.80	.488	9.97	.311	4350	412	2.94	2001	3.10
39	17.61	.491	10.00	.367	1009	1198	8.56	231	3.67
40	20.85	.480	10.19	.273	1195	1023	7.31	292	2.78
41	25.82	.483	9.99	.245	1480	865	6.18	406	2.45
42	29.81	.482	9.90	.230	1708	772	5.52	510	2.28
43	34.42	.485	9.90	.238	1973	696	4.97	631	2.36
44	36.72	.490	10.00	.226	2104	669	4.78	690	2.26
45	46.25	.487	10.00	.251	2650	566	4.04	983	2.51
46	55.22	.482	10.00	.276	3165	498	3.56	1276	2.76
47	67.70	.473	10.00	.314	3880	434	3.09	1716	3.14
48	82.00	.484	10.00	.360	4700	392	2.80	2210	3.60
49	13.35	.481	10.03	.532	764	1495	10.68	150	5.34
50	15.40	.483	9.98	.420	882	1325	9.47	184	4.19
51	16.00	.485	9.90	.371	917	1289	9.21	195	3.68
52	16.86	.627	10.10	.564	967	1530	10.93	188	5.70
53	19.20	.640	10.00	.465	1100	1384	9.89	225	4.65
54	22.15	.638	10.00	.390	1270	1204	8.60	281	3.90
55	26.97	.626	9.94	.347	1546	1023	7.31	382	3.45
56	32.80	.630	9.92	.310	1880	882	6.30	504	3.08
57	38.80	.626	10.00	.295	2225	768	5.49	664	2.95
58	45.20	.636	10.00	.300	2590	695	4.97	827	3.00
59	93.40	.653	9.98	.481	5360	433	3.09	2365	4.79
60	21.60	.646	10.00	.445	1238	1273	9.09	263	4.45
61	25.60	.651	10.00	.357	1467	1106	7.90	334	3.57
62	31.10	.644	10.00	.329	1782	938	6.70	455	3.29
63	39.20	.646	9.98	.319	2247	785	5.61	662	3.18
64	43.70	.647	10.00	.318	2505	722	5.16	768	3.18
65	54.20	.643	10.00	.338	3105	615	4.39	1083	3.38
66	65.20	.639	10.00	.378	3740	539	3.82	1410	3.78
67	76.00	.642	9.96	.430	4355	488	3.49	1758	4.28
68	72.20	.642	10.00	.435	4140	503	3.40	1705	4.35
69	62.00	.659	10.00	.370	3550	565	4.04	1295	3.70
70	37.50	.654	9.82	.335	2150	821	5.87	618	3.29
71	16.80	.631	9.90	.657	962	1552	11.08	184	6.50
72	18.20	.633	9.93	.548	1042	1450	10.35	208	5.44
73	90.00	.642	9.96	.535	5160	439	3.13	2260	5.33

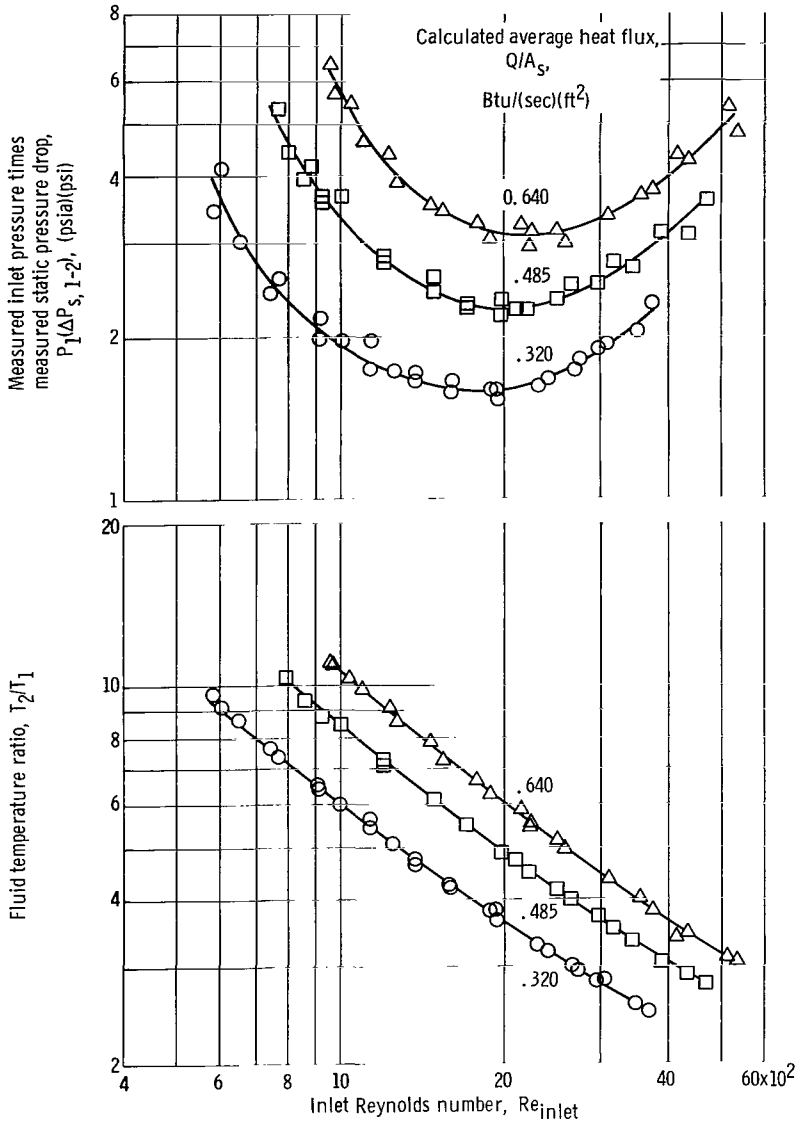

Figure 6. - Experimental static pressure drop and experimental fluid temperature ratio against inlet Reynolds number with heat flux as a parameter.

In figure 6, no distinction is made between the data points obtained from the initial set of test runs and those obtained from the two sets of reruns. In general, no significant difference was observed between the initial test run data and that obtained from the reruns; hence, it appears that the test points are reasonably reproducible.

A summary of the measured and calculated data for each test run is presented in table II. An inspection of these data shows the experimental heat-flux value for each test run to be within ±3 percent of the reported nominal values. The procedure used in calculating the values in table II is demonstrated in appendix C by a sample calculation.

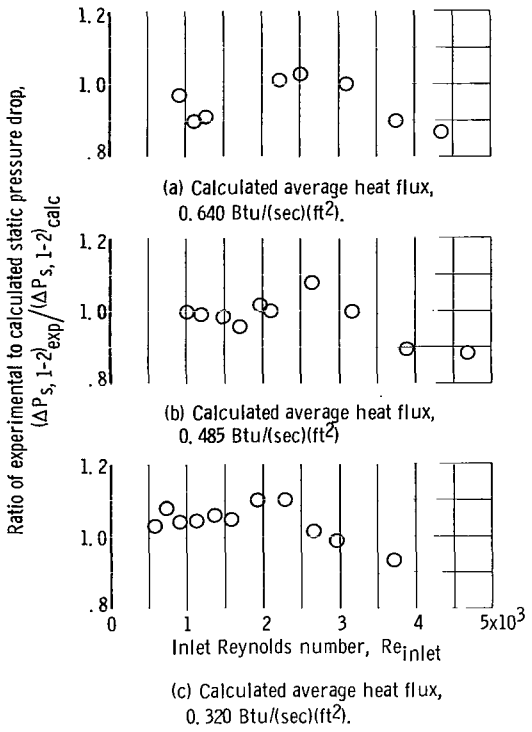

Figure 7. - Comparison of experimental and calculated pressure-drop values for three operating heat fluxes.

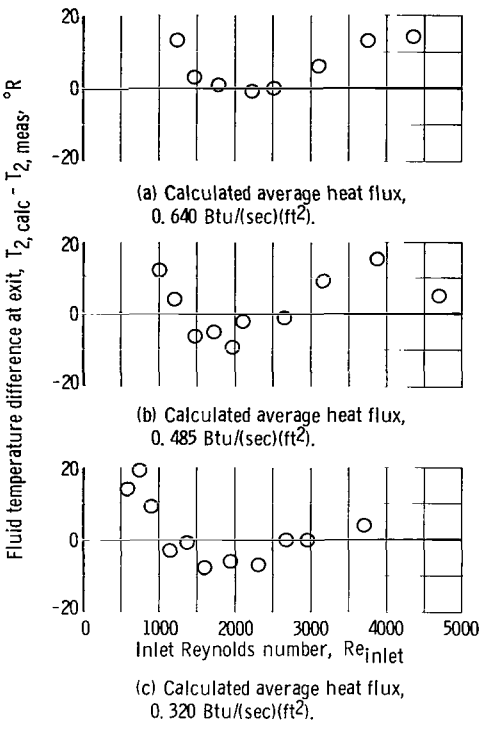

Figure 8. - Comparison of experimental and calculated fluid temperatures at test-section exit for three operating heat fluxes.

Comparison of Experimental and Calculated Pressure Drops

The calculated pressure drops for several test runs made at each of the three operating heat fluxes were compared with the respective measured pressure-drop values; the results of this comparison are shown in figure 7. The assumptions, equations, and analytical procedures employed in the calculations are described in the section PRESSURE-DROP ANALYSIS. As mentioned in the section EXPERIMENTAL APPARATUS AND PROCEDURE, wall temperature measurements were not obtained for all of the experimental runs because of thermocouple failures. As a result, pressure drops for all test runs could not be computed.

Figure 7 shows that with the exception of a few points, the calculated pressure-drop values agree with the experimental values within about ±10 percent. The differences between the experimental and calculated pressure drops for the three different operating heat fluxes appear to follow no consistent pattern.

In these experiments, no measurements were taken of local fluid temperatures along the length of the heated passage. As a result, the calculated fluid temperature profiles and heat-flux profiles could not be experimentally validated. Fluid temperature measurements taken at the exit of the test section did, however, compare rather closely with the calculated outlet fluid temperatures.

Figure 8 shows the differences between the calculated and measured values

of exit fluid temperatures for the test runs analyzed. From figure 8, it is seen that with the exception of one of the test runs, the experimental and calculated fluid temperatures at the test section exit agree within ±15° R.

In judging the comparison between experimental and calculated pressure drops in figure 7, it should be recalled that the computed pressure-drop values were dependent on the heat-transfer relations used as well as the pressure drop relations.

Nevertheless, the experimental and calculated values of pressure drop for the individual test runs are reasonably close. The data in figure 7 indicate that the pressure-drop and heat-transfer relations along with the assumed flow transition criterion used in the analysis were reasonable.

DISCUSSION OF TEST DATA

Some idea of the large flow and temperature nonuniformities possible in a system of parallel flow passages can be seen from an examination of figure 6. For example, the curve constructed through the data points for the average heat flux of 0.640 Btu/(sec)(ft^2) shows that for a value of $P_1 \Delta P_{s,1-2}$ of 4.5, the flow rates and/or inlet Reynolds numbers that satisfy these conditions may differ by a factor of approximately four. The corresponding outlet fluid temperatures for the two flow rates differ by approximately 900° R.

The large flow and temperature differences cited in the preceding example are based on the assumption that each of the parallel flow passages is thermally isolated from the other flow passages in the system. In the solid core of the nuclear rocket, the magnitude of the nonuniformities in flow and temperature would be reduced by heat conduction between adjacent fuel cells. If the heat interchange by conduction between fuel cells is large enough to prevent thermal damage in the core, the problem of laminar-flow instability (as applied to the solid core of the nuclear rocket) may be of little significance. The uncertainty in the conduction contact resistance between the fuel cells in the reactor core makes it impossible to estimate accurately the effectiveness of radial heat conduction in preventing temperature and flow maldistributions of the type associated with the laminar instability phenomenon.

Therefore, the magnitude of possible nonuniformities cited in the preceding example should be carefully interpreted. Application of these data and conclusions drawn regarding possible nonuniformities of temperature and flow among parallel flow passages is justified only where the effect of thermal coupling between channels is negligible.

CONCLUDING REMARKS

Since gas-cooled nuclear reactors are normally designed for operation in the turbulent flow regime, the laminar-flow instability phenomenon reported herein would not appear to present a problem for steady-state design operation. During the startup and shutdown of a gas-cooled reactor, the system flow rate must pass through the laminar flow regime. In the case of shutdown, the re-

actor decay heat may be sufficiently large to require cooling of the core assembly for relatively long periods of time. If coolant consumption is to be minimized during the period of afterheat removal (as would be required for the missions being considered for the nuclear rocket), it is necessary that the flow rate be controlled to a minimum value which would maintain the core assembly slightly below the maximum allowable temperature.

The experimental data presented in this report show that a heated flow channel operating at steady state with a constant heat flux may have two widely different flow rates which yield the same value of pressure drop. As a result, it seems reasonable to expect that nonuniformities of temperature and flow could occur in a system of uniformly heated parallel flow passages operating at low flow rates between fixed pressure boundaries.

For the range of test conditions investigated, the experimental data indicate that

1. The slopes of the curves of pressure drop against flow rate and/or inlet Reynolds number are negative for outlet-to-inlet fluid temperature ratios greater than 5.5.

2. The flow rate (or inlet Reynolds number) corresponding to the point of minimum pressure drop increases with increasing values of heat flux. At the lowest heat flux, the relative minimum pressure drop occurred at an inlet Reynolds number of approximately 1800; at the highest heat flux, the relative minimum pressure drop occurred at an inlet Reynolds number of approximately 2300.

Several test runs were made at each average operating heat flux to investigate the reproducibility of the experimental measurements. In general, the experimental pressure-drop measurements were reproducible, even in the regime of mixed flow.

A comparison was made of experimental and calculated values of pressure drop in the heated flow passage. Fluid temperature profiles required for the pressure-drop analysis were estimated from a convection heat-transfer analysis in which measured values of the wall temperature distributions were used. An assumed turbulent-to-laminar flow transition criterion was used in the pressure-drop heat-transfer analysis to compute axial fluid temperature distributions for those test runs having mixed flow. The agreement in experimental and calculated values of pressure drop indicates that the heat-transfer and pressure-drop relations along with the assumed flow transition criterion were reasonable.

Lewis Research Center,
National Aeronautics and Space Administration,
Cleveland, Ohio, November 23, 1965.

APPENDIX A

SYMBOLS

A	flow area, ft^2
A_s	inside surface area of test section, ft^2
C_p	specific heat of gas at constant pressure, Btu/(lb)(^oR)
D_H	hydraulic diameter of test section, ft
f	friction factor
f_o	constant in friction factor equation (eq. (B5))
g	gravitational constant, $ft/(sec)^2$
H	enthalpy, Btu/lb
h_x	local heat-transfer coefficient, Btu/(sec)(ft^2)(^oR)
k	thermal conductivity of gas, Btu/(sec)(ft)(^oR)
L	heat-transfer length of test section, ft
M	exponent on temperature in viscosity relation (eq. (B6))
n	exponent on Reynolds number in friction factor relation (eq. (B5))
P, P_s	static pressure, psia (except in appendix B where psfa is used)
Pr	Prandtl number, $\mu C_p/k$
Q	rate of heat transfer to gas, Btu/sec
R	specific gas law constant, $ft/^oR$
Re	Reynolds number, $\dot{w}D_H/A\mu$
T	temperature, ^oR
v	fluid velocity, ft/sec
$\dot{w}$	weight flow rate, lb/sec
x	axial distance from inlet of test section, ft
μ	viscosity, lb/(ft)(sec)

μ_o constant coefficient in viscosity relation (eq. (B6))

τ outlet-to-inlet fluid temperature ratio, T_2/T_1

Subscripts:

ave average

b bulk (when applied to fluid properties, indicates evaluation based on bulk temperature)

crit critical

f film (when applied to fluid properties, indicates evaluation based on film temperature, $T_f = (T_{wall} + T_b)/2$)

wall inside surface of test section

x local value at distance x from test-section inlet

1 test-section inlet

2 test-section outlet

APPENDIX B

APPROXIMATE CLOSED-FORM PRESSURE DROP-FLOW ANALYSIS

Consider a heated flow channel of length L in which a fluid flowing at a rate $\dot{w}$ enters the channel at temperature T_1 and pressure P_1 and leaves the channel at temperature T_2 and pressure P_2 as shown in figure 9. If changes in potential energy of the fluid are neglected, the static pressure drop across the heated flow channel $\Delta P_{s,1-2}$ is given by the following equation:

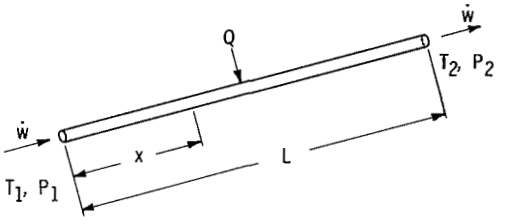

Figure 9. - Heated flow channel.

$$\Delta P_{s,1-2} = \Delta P_{momentum} + \Delta P_{friction} \tag{B1}$$

If the fluid is assumed to behave as a perfect gas and if the pressure-drop is small relative to the inlet pressure,

$$\Delta P_{momentum} = 2\left(\frac{\dot{w}}{A}\right)^2 \frac{R}{g} \frac{1}{P_1 + P_2}\left(T_2 - T_1\right) \tag{B2}$$

$$\Delta P_{friction} = \frac{4}{D_H}\left(\frac{\dot{w}}{A}\right)^2 \frac{R}{g} \frac{1}{P_1 + P_2} \int_{x=0}^{x=L} fT\, dx \tag{B3}$$

Hence, equation (B1) may be written as

$$\Delta P_{s,1-2} = 2\left(\frac{\dot{w}}{A}\right)^2 \frac{R}{g} \frac{1}{P_1 + P_2}\left(T_2 - T_1 + \frac{2}{D_H} \int_{x=0}^{x=L} fT\, dx\right) \tag{B4}$$

The friction factor f in equations (B3) and (B4) is expressed as a function of the local Reynolds number Re_x by

$$f = \frac{f_o}{Re_x^n} = \frac{f_o}{\left(\frac{\dot{w} D_H}{A \mu_x}\right)^n} = \frac{f_o \mu_x^n}{\left(\frac{\dot{w}}{A} D_H\right)^n} \tag{B5}$$

For laminar flow (ref. 7),

$$f_o = \text{constant} = 16$$

$$n = 1.0$$

For turbulent flow (ref. 7)

$$f_o = 0.046$$

$$n = 0.2$$

The local fluid viscosity μ_x is represented as a function of the local fluid temperature T by

$$\mu_x = \mu_o T^M \tag{B6}$$

Combining equations (B4), (B5), and (B6) yields

$$\Delta P_{s,1-2} = 2\left(\frac{\dot{w}}{A}\right)^2 \frac{R}{g} \frac{1}{P_1 + P_2}\left[T_2 - T_1 + \frac{2}{D_H} \frac{f_o \mu_o^n}{\left(\frac{\dot{w}}{A} D_H\right)^n} \int_{x=0}^{x=L} T^{Mn+1}\, dx\right] \tag{B7}$$

If the Mach number in the heated channel is small relative to one, the static temperature rise of the fluid is related to the heat input by

$$Q = \dot{w} \int_{T_1}^{T_2} C_p\, dT \tag{B8}$$

Integrating equation (B8) (assuming C_p constant) and rearranging give

$$T_2 - T_1 = \frac{Q}{\dot{w} C_p} \tag{B9}$$

(For normal hydrogen gas, the assumption that C_p is constant is rather poor at temperatures below about 500° R.)

For a constant diameter channel, the surface area for heat transfer is

$$A_s = \pi D_H L \tag{B10}$$

Multiplying numerator and denominator of the right side of equation (B9) by $A_s = \pi D_H L$ gives

$$T_2 - T_1 = \frac{Q \pi D_H L}{A_s \dot{w} C_p} \tag{B11}$$

The flow area of a circular channel is $A = (\pi/4)(D_H)^2$; hence,

$$\pi = 4A/(D_H)^2$$

Substitution of $4A/(D_H)^2$ for π in equation (B11) gives

$$T_2 - T_1 = \frac{4QL}{A_s C_p D_H \left(\frac{\dot{w}}{A}\right)} \tag{B12a}$$

If the heat flux is defined as Q/A_s and the heat input is assumed to be uniformly distributed along the length of the channel (such that $(Q/A_s)_{ave} = (Q/A_x)_x$), equation (B12a) may be written as

$$T - T_1 = \frac{4Qx}{A_s C_p D_H \left(\frac{\dot{w}}{A}\right)} \tag{B12b}$$

The integral in equation (B7) is evaluated as follows:

$$\int_{x=0}^{x=L} T^{Mn+1}\, dx = \int_{x=0}^{x=L} \left[T_1 + \frac{4Qx}{A_s C_p D_H \left(\frac{\dot{w}}{A}\right)}\right]^{Mn+1} dx \tag{B13a}$$

$$\int_{x=0}^{x=L} T^{Mn+1}\, dx = \frac{1}{Mn+2} \frac{A_s C_p D_H \frac{\dot{w}}{A}}{4Q} \left(T_1 + \frac{4Qx}{A_s C_p D_H \frac{\dot{w}}{A}}\right)^{Mn+2} \Bigg|_{x=0}^{x=L} \tag{B13b}$$

$$\int_{x=0}^{x=L} T^{Mn+1}\, dx = \frac{1}{Mn+2} \frac{A_s C_p D_H \frac{\dot{w}}{A}}{4Q} \left[\left(T_1 + \frac{4QL}{A_s C_p D_H \left(\frac{\dot{w}}{A}\right)}\right)^{Mn+2} - T_1^{Mn+2}\right] \tag{B13c}$$

Combining equations (B12a) and (B13c) yields

$$\int_{x=0}^{x=L} T^{Mn+1}\, dx = \frac{L}{(Mn+2)(T_2 - T_1)} \left(T_2^{Mn+2} - T_1^{Mn+2}\right) \tag{B13d}$$

Substituting the result of equation (B13d) into equation (B7) gives

$$\Delta P_{s,1\text{-}2} = 2 \frac{R}{g} \frac{1}{P_1 + P_2} \left(\frac{\dot{w}}{A}\right)^2 \left[T_2 - T_1 + \frac{2}{D_H} \frac{f_o \mu_o^n}{\left(\frac{\dot{w}}{A} D_H\right)^n} \frac{L}{(Mn+2)(T_2 - T_1)} \left(T_2^{Mn+2} - T_1^{Mn+2}\right)\right] \tag{B14}$$

Multiplying numerator and denominator of equation (B14) by T_1,

$$\Delta P_{s,1-2} = 2\frac{R}{g}\frac{T_1}{P_1 + P_2}\left(\frac{\dot{w}}{A}\right)^2\left\{\frac{T_2 - T_1}{T_1} + \frac{2f_o\mu_o^n L T_1^{Mn+2}}{D_H\left(\frac{\dot{w}}{A}D_H\right)^n (Mn + 2)T_1(T_2 - T_1)}\left[\left(\frac{T_2}{T_1}\right)^{Mn+2} - 1\right]\right\} \quad \text{(B15a)}$$

From equation (B6), $\mu_x = \mu_o T^M$; hence,

$$\mu_1^n = \mu_o^n T_1^{Mn} \quad \text{(B15b)}$$

Substituting the result of (B15b) into (B15a) gives

$$\Delta P_{s,1-2} = 2\frac{R}{g}\frac{T_1}{P_1 + P_2}\left(\frac{\dot{w}}{A}\right)^2\left\{\frac{T_2 - T_1}{T_1} + \frac{2f_o\mu_1^n L T_1}{D_H\left(\frac{\dot{w}}{A}D_H\right)^n (Mn + 2)(T_2 - T_1)}\left[\left(\frac{T_2}{T_1}\right)^{Mn+2} - 1\right]\right\} \quad \text{(B16)}$$

Combining equation (B12a) with (B16)

$$\Delta P_{s,1-2} = \frac{2R}{g}\frac{T_1}{P_1 + P_2}\left(\frac{\dot{w}}{A}\right)^2\left\{\frac{4QL}{A_s C_p D_H T_1 \frac{\dot{w}}{A}} + \frac{2}{D_H}\frac{f_o\mu_1^n L}{\left(\frac{\dot{w}}{A}D_H\right)^n (Mn + 2)}\frac{A_s C_p D_H T_1 \frac{\dot{w}}{A}}{4QL} \times \left[\left(1 + \frac{4QL}{A_s C_p D_H T_1 \frac{\dot{w}}{A}}\right)^{Mn+2} - 1\right]\right\} \quad (1)$$

Equation (1) is the general equation of the family of curves shown in figure 1.

Taking the partial derivative of $\Delta P_{s,1-2}$ with respect to $\dot{w}/A$ at a constant heat flux shows that a relative minimum exists for the curves in figure 1.

$$\left.\frac{\partial\,\Delta P_{s,1\text{-}2}}{\partial\left(\frac{\dot{w}}{A}\right)}\right|_{Q/A_s} = 2\,\frac{R}{g}\,\frac{T_1}{P_1 + P_2}\left\{\frac{4QL}{A_s D_H C_p T_1} + \frac{2f_o\mu_1^n LA_s D_H C_p T_1\left(\frac{\dot{w}}{A}\right)^3}{4QLD_H\left(\frac{\dot{w}}{A}\,D_H\right)^n}\right.$$

$$\times\left(1 + \frac{4QL}{A_s C_p D_H T_1\,\frac{\dot{w}}{A}}\right)^{Mn+1}\left[-\frac{4QL}{A_s C_p D_H T_1\left(\frac{\dot{w}}{A}\right)^2}\right] + \frac{2f_o\mu_1^n LA_s D_H C_p T_1}{4QLD_H(Mn+2)}$$

$$\times\left(1 + \frac{4QL}{A_s D_H C_p T_1\,\frac{\dot{w}}{A}}\right)^{Mn+2}\left[\frac{(3-n)\left(\frac{\dot{w}}{A}\right)^2}{\left(D_H\,\frac{\dot{w}}{A}\right)^n}\right]$$

$$\left. - \frac{2f_o\mu_1^n LA_s D_H C_p T_1}{4QLD_H(Mn+2)}\left[\frac{(3-n)\left(\frac{\dot{w}}{A}\right)^2}{\left(D_H\,\frac{\dot{w}}{A}\right)^n}\right]\right\} \qquad \text{(B17)}$$

Simplifying equation (B17) by virtue of equations (B5) and (B12a) gives

$$\left.\frac{\partial\,\Delta P_{s,1\text{-}2}}{\partial\left(\frac{\dot{w}}{A}\right)}\right|_{Q/A_s} = 2\,\frac{R}{g}\,\frac{T_1}{P_1 + P_2}\left\{\frac{4QL}{A_s C_p D_H T_1} + \frac{2f_1 LT_1\left(\frac{\dot{w}}{A}\right)^2}{D_H(T_2 - T_1)}\right.\left(1 + \frac{T_2 - T_1}{T_1}\right)^{Mn+1}$$

$$\times\left(-\frac{1}{\frac{\dot{w}}{A}}\,\frac{T_2 - T_1}{T_1}\right) + \frac{2f_1 LT_1}{D_H(Mn+2)(T_2 - T_1)}\left[(3-n)\frac{\dot{w}}{A}\right]\left(1 + \frac{T_2 - T_1}{T_1}\right)^{Mn+2}$$

$$\left. - \frac{2f_1 LT_1}{D_H(Mn+2)(T_2 - T_1)}\left[(3-n)\frac{\dot{w}}{A}\right]\right\} \qquad \text{(B18)}$$

Let $\tau = T_2/T_1$; then equation (B18) becomes

$$\left.\frac{\partial\,\Delta P_{s,1\text{-}2}}{\partial\left(\frac{\dot{w}}{A}\right)}\right|_{Q/A_s} = 2\,\frac{R}{g}\,\frac{T_1}{P_1 + P_2}\left\{\frac{4QL}{A_s C_p D_H T_1} + \frac{2f_1 L\,\frac{\dot{w}}{A}}{D_H(\tau - 1)}\,\tau^{Mn+1}\left[-(\tau - 1)\right]\right.$$

$$\left. + \frac{2f_1 L(3-n)\frac{\dot{w}}{A}\,\tau^{Mn+2}}{D_H(Mn+2)(\tau - 1)} - \frac{2f_1 L(3-n)\frac{\dot{w}}{A}}{D_H(Mn+2)(\tau - 1)}\right\} \qquad \text{(B19)}$$

Simplifying equation (B19) gives

$$\left.\frac{\partial\,\Delta P_{s,1-2}}{\partial\left(\frac{\dot{w}}{A}\right)}\right|_{Q/A_s} = 2\,\frac{R}{g}\,\frac{T_1}{P_1 + P_2}\left\{\frac{4QL}{A_s C_p D_H T_1} + \frac{2f_1 L\,\frac{\dot{w}}{A}\,\tau^{Mn+1}}{D_H}\right.$$

$$\left.\times\left[-1 + \frac{(3-n)\tau}{(Mn+2)(\tau-1)} - \frac{(3-n)}{(Mn+2)(\tau-1)\tau^{Mn+1}}\right]\right\} \qquad (B20)$$

Combining equations (B12a) and (B20) yields

$$\left.\frac{\partial\,\Delta P_{s,1-2}}{\partial\left(\frac{\dot{w}}{A}\right)}\right|_{Q/A_s} = 2\,\frac{R}{g}\,\frac{T_1}{P_1 + P_2}\,\frac{\dot{w}}{A}\left\{\tau - 1 + \frac{2f_1 L\tau^{Mn+1}}{D_H}\right.$$

$$\left.\times\left[-1 + \frac{3-n}{Mn+2}\left(\frac{\tau}{\tau-1} - \frac{1}{(\tau-1)\tau^{Mn+1}}\right)\right]\right\} \qquad (B21)$$

The minimum of the curves of $\Delta P_{s,1-2}$ against $\dot{w}/A$ occurs at a point where $\partial\,\Delta P_{s,1-2}/\partial(\dot{w}/A) = 0$; hence, the sum of the terms inside the braces of equation (B21) must equal zero for a minimum to exist.

For most gases, the viscosity varies with the temperature to powers of less than one; that is, $\mu = \mu_o T^M$, where $M < 1.0$.

For hydrogen gas in the range from 150° to 1500° R, M is approximately 0.72.

If the flow in the heated passage is completely turbulent (such that $n \cong 0.2$, it can be shown that $\partial\,\Delta P_{s,1-2}/\partial(\dot{w}/A)\big|_{Q/A_s}$ is always positive.

For laminar flow throughout the heated passage, $n = 1.0$. Assuming a ratio L/D_H of 430, $\partial\,\Delta P_{s,1-2}/\partial(\dot{w}/A)\big|_{Q/A_s}$ in equation (B21) changes from positive to negative for laminar flow at a value of τ of approximately 4.0. The exact value of τ_{crit} (i.e., the value of τ at which $\partial\,\Delta P_{s,1-2}/\partial(\dot{w}/A)\big|_{Q/A_s} = 0$) is dependent on the ratio L/D_H, the heat-flux value, the inlet fluid temperature, and the flow rate.

APPENDIX C

SAMPLE CALCULATION

The following sample calculation (run 30) shows the procedure used to obtain the calculated values in table II:

Inlet static pressure, $P_{s,1}$, psia	9.87
Inlet hydrogen gas temperature, T_1, $^{\circ}R$	140
Hydrogen gas flow rate, $\dot{w}$, lb/sec	20.91×10^{-6}
Outlet hydrogen gas temperature, T_2, $^{\circ}R$	1004
Inlet to exit static pressure drop, $\Delta P_{s,1-2}$, psi	0.289

(a) Calculation of Reynolds number at test section inlet

Tube diameter

$$D_H = 0.116 \text{ in.} = 9.667 \times 10^{-3} \text{ ft}$$

Tube flow area

$$A = (\pi/4)(0.116)^2 = 0.010565 \text{ in.}^2 = 7.34 \times 10^{-5} \text{ ft}^2$$

Viscosity of normal hydrogen gas (ref. 15) at test section inlet

$$\mu_1 = 2.3 \times 10^{-6} \text{ lb/(ft)(sec)}$$

Inlet Reynolds number

$$Re_{inlet} = \frac{\dot{w} D_H}{A \mu_1} = \frac{(20.91 \times 10^{-6})(9.667 \times 10^{-3})}{(7.34 \times 10^{-5})(2.3 \times 10^{-6})}$$

Inlet Reynolds number

$$Re_{inlet} \cong 1200$$

(b) Calculation of average heat flux

Surface area of tube

$$A_s = \pi D_H L = \frac{\pi(0.116)(50)}{144} \equiv 0.1265 \text{ ft}^2$$

Rate of heat transfer to fluid

$$Q = \dot{w} \int_{T_1}^{T_2} C_p \, dT = \dot{w}(H_2 - H_1)$$

From reference 15

$$H_2 = f(T_2, P_2) = 3425 \text{ Btu/lb}$$

$$H_1 = f(T_1, P_1) = 573 \text{ Btu/lb}$$

Rate of heat transfer to fluid

$$Q = 20.91 \times 10^{-6} \ (3425-573) = 5.955 \times 10^{-2} \text{ Btu/sec}$$

Average heat flux

$$\frac{Q}{A_s} = \frac{5.955 \times 10^{-2}}{0.1265} = 0.472 \text{ Btu/(sec)(ft}^2\text{)}$$

(c) Calculation of Reynolds number at test section outlet

Viscosity of normal hydrogen gas (ref. 15) at test section outlet

$$\mu_2 = 9.1 \times 10^{-6} \text{ lb/(ft)(sec)}$$

$$Re_{outlet} = Re_{inlet} \frac{\mu_1}{\mu_2}$$

$$Re_{outlet} = 1200 \frac{2.3 \times 10^{-6}}{9.1 \times 10^{-6}} \cong 300$$

(d) Calculation of fluid temperature ratio

Fluid temperature ratio

$$\tau = \frac{T_2}{T_1} = \frac{1004}{140} = 7.17$$

(e) Calculation of pressure-drop parameter

$$P_1 \ \Delta P_{s,1-2} = (9.87)(0.289) = 2.85(\text{psia})(\text{psi})$$

REFERENCES

1. Ellerbrock, Herman H.; Livingood, John N. B.; and Straight, David M.: Fluid-Flow and Heat-Transfer Problems in Nuclear Rockets. Proceedings of the NASA-University Conference on the Science and Technology of Space Exploration, vol. 2, NASA SP-11, 1962, pp. 87-116. (Also available as NASA SP-2a)

2. Bussard, R. W.; and De Lauer, R. D.: Nuclear Rocket Propulsion. McGraw-Hill Book Co., Inc., 1958.

3. Gruber, Alan R.; and Hyman, Seymour C.: Flow Distribution Among Parallel Heated Channels. A.I.Ch.E. J., vol. 2, no. 2, June 1956, pp. 199-205.

4. Connolley, T. J.: Temperature and Flow Distribution Among the Channels of a Rocket-Propulsion Nuclear Reactor. Rep.-B061266, Lockheed Missiles and Space Co., Jan. 25, 1963.

5. Guevara, F. A.; McInteer, B. B.; and Potter, R. M.: Temperature-Flow Stability Experiments. Report LAMS-2934, Los Alamos Scientific Lab, Aug. 30, 1963.

6. Harry, David P., III: A Steady-State Analysis of the "Laminar-Instability" Problem Due to Heating Para-Hydrogen in Long, Slender Tubes. NASA TN D-2084, 1964.

7. McAdams, William H.: Heat Transmission. Third ed., McGraw-Hill Book Co., Inc., 1954.

8. Turney, George E.: An Experimental Investigation of the "Laminar Flow Instability" Problem Related to the Strong Heating of Normal-Hydrogen Gas in a Small Diameter Tube. M.S. Thesis, Univ. of Cincinnati, 1965.

9. Staff of the Lewis Research Center: A Central Facility for Recording and Processing Transient-Type Data. NASA TN D-1320, 1963.

10. Davenport, M. E.; and Leppert, G.: The Effect of Transverse Temperature Gradients on the Heat Transfer and Friction for Laminar Flow of Gases. Paper No. 64-HT-10, ASME, Aug. 1964.

11. Knudsen, James G.: Fluid Dynamics and Heat Transfer. McGraw-Hill Book Co., Inc., 1958.

12. Kays, W. M.: Numerical Solutions for Laminar-Flow Heat Transfer in Circular Tubes. Paper No. 54-A-151, ASME, Nov.-Dec. 1954.

13. Kreith, Frank: Principles of Heat Transfer. International Textbook Co., 1958.

14. Vennard, John K.: Elementary Fluid Mechanics. Third ed., John Wiley & Sons, Inc., 1954.

15. Harry, David P., III: Formulation and Digital Coding of Approximate Hydrogen Properties for Application to Heat-Transfer and Fluid-Flow Computations. NASA TN D-1664, 1963.

"The aeronautical and space activities of the United States shall be conducted so as to contribute . . . to the expansion of human knowledge of phenomena in the atmosphere and space. The Administration shall provide for the widest practicable and appropriate dissemination of information concerning its activities and the results thereof."

—NATIONAL AERONAUTICS AND SPACE ACT OF 1958

NASA SCIENTIFIC AND TECHNICAL PUBLICATIONS

TECHNICAL REPORTS: Scientific and technical information considered important, complete, and a lasting contribution to existing knowledge.

TECHNICAL NOTES: Information less broad in scope but nevertheless of importance as a contribution to existing knowledge.

TECHNICAL MEMORANDUMS: Information receiving limited distribution because of preliminary data, security classification, or other reasons.

CONTRACTOR REPORTS: Technical information generated in connection with a NASA contract or grant and released under NASA auspices.

TECHNICAL TRANSLATIONS: Information published in a foreign language considered to merit NASA distribution in English.

TECHNICAL REPRINTS: Information derived from NASA activities and initially published in the form of journal articles.

SPECIAL PUBLICATIONS: Information derived from or of value to NASA activities but not necessarily reporting the results of individual NASA-programmed scientific efforts. Publications include conference proceedings, monographs, data compilations, handbooks, sourcebooks, and special bibliographies.

Details on the availability of these publications may be obtained from:

SCIENTIFIC AND TECHNICAL INFORMATION DIVISION

NATIONAL AERONAUTICS AND SPACE ADMINISTRATION

Washington, D.C. 20546